Spectroscopic Studies on the Designed Metal-Binding Sites of the 43C9 Single Chain Antibody†

Michael W. Crowder,‡ Jon D. Stewart,‡,§ Victoria A. Roberts,⊥ Christopher J. Bender,∥ Eugene Tevelrakh,¶ Jack Peisach,∥ Elizabeth D. Getzoff,⊥ Betty J. Gaffney,× and Stephen J. Benkovic*,‡

Contribution from the Department of Chemistry, 152 Davey Laboratory, The Pennsylvania State University, University Park, Pennsylvania 16802, Department of Molecular Biology, The Scripps Research Institute, 10666 North Torrey Pines Road, La Jolla, California 92037, Departments of Molecular Pharmacology and Physiology, Albert Einstein College of Medicine of Yeshiva University, Bronx, New York 10461, and Departments of Chemistry and Biophysics, Johns Hopkins University, Baltimore, Maryland 21228

Received November 4, 1994⊗

Abstract: In an effort to expand the catalytic repertoire of antibodies to encompass metal ion-assisted reactions, three classes of metal ion-binding sites were designed within the antigen-binding site of catalytic single-chain antibody (SCA) 43C9 and characterized by a variety of spectroscopic techniques. With structural motifs of metalloenzymes as prototypes, computer modeling techniques were used to design these sites. The affinities of each class of metal ion-binding sites for a variety of divalent metal ions were determined by fluorescence quenching techniques. One class of binding sites, consisting of His residues at positions L32, L34, and L91, bound Zn(II) with a K_D value of 3.3 ± 0.8 μM; however, the affinity for the inducing antigen was decreased by at least 10^4 relative to that of the wild-type in the absence of Zn(II). The second class of metal ion-binding sites, which consisted of His residues at positions H33, H35, and H95, possessed greater than 100-fold selectivity for Zn(II) over any other divalent metal ion tested and bound this ion with K_D values of 1.5−3.7 μM. The third class of metal ion-binding sites utilized His residues at positions L91 and L96 and, in some cases, H95. This class was selective for Cu(II) over Zn(II), binding the former with K_D values of 0.5−2.1 μM and the latter with K_D values of 10−40 μM. Continuous-wave EPR studies of Cu(II) bound to this class of mutants verified the results of the fluorescence quenching assays; Cu(II) binding resulted in EPR signals that were well approximated by a simulation using the parameters of $A_{\|}$ = 166.0G, $A_{\perp}$ = 6.0G, $g_{\|}$ = 2.19, and $g_{\perp}$ = 2.05. Furthermore, pulsed EPR experiments (ESEEM) demonstrated that (1) a low-affinity Cu(II) site ($K_D \geq 100$ μM) consisting of a single His residue existed in the wild-type SCA, (2) two His residues acted as Cu(II) ligands in the R-L96-H single mutant, and (3) three His residues acted as Cu(II) ligands in the R-L96-H, Y-H95-H double mutant. These results are consistent with the original computational design. In addition, UV−vis studies suggested a rare Tyr to Cu(II), ligand-to-metal charge transfer band at 490 nm (ϵ = 55 M^{-1} cm^{-1}) that arose from coordination of the Tyr H95 side chain to the bound Cu(II). As expected, this band was absent in the Cu(II)-bound form of the R-L96-H, Y-H95-F double mutant SCA. Finally, the R-L96-H mutant was shown to simultaneously bind metal and *p*-nitrophenol.

Introduction

Although over 60 chemical reactions have been shown to be catalyzed by antibodies,[1] two problems have plagued the antibody field's goal of using these tailor-made reactivities as biomedical therapies. The first is that almost all known catalytic antibodies have modest catalytic efficiencies (i.e., low turnover numbers), and the second is that there is no successful approach for delivering catalysts to a desired *in vivo* destination. Four major strategies have been employed to address the first problem: (1) increasing the number of candidates by screening large combinatorial libraries of antibodies,[2] (2) improving hapten design to provide better transition state mimics,[1b] (3) integrating results of modeling and mechanistic studies with site-directed mutagenesis to rationally improve catalytic turnover,[3] and (4) incorporating metal ions into antigen-binding sites.[4] We have been interested in antibody-catalyzed hydrolytic reactions and

* To whom correspondence should be addressed.

† Abbreviations: *A*, electron-nuclear hyperfine constant; CDR, complementary determining region; [Cu(II)$_T$], total Cu(II) concentration; CW, continuous wave; EDTA, ethylenediaminetetraacetic acid; EPR, electron paramagnetic resonance; ESEEM, electron spin echo envelope modulation; ϵ, molar extinction coefficient; FT, Fourier transform; G, gauss; HEPES, (*N*-[2-hydroxyethyl]piperazine-*N*'-[2-ethanesulfonic acid]); H, heavy chain; *I*, nuclear spin; K_D, thermodynamic dissociation constant; L, light chain; LMCT, ligand to metal charge transfer, SCA, single chain antibody; *S*, electron spin.

‡ The Pennsylvania State University.
§ Present address: Department of Chemistry, University of Florida, Gainesville, FL 19126.
⊥ The Scripps Research Institute.
∥ Yeshiva University.
¶ Department of Biophysics, Johns Hopkins University.
× Department of Chemistry, Johns Hopkins University.

⊗ Abstract published in *Advance ACS Abstracts*, May 1, 1995.

(1) (a) Lerner, R. A.; Benkovic, S. J.; Schultz, P. G. *Science* **1991**, *252*, 659. (b) Stewart, J. D.; Liotta, L. J.; Benkovic, S. J. *Acc. Chem. Rev.* **1993**, *26*, 396. (c) Benkovic, S. J. *Annu. Rev. Biochem.* **1992**, *61*, 29.

(2) Posner, B.; Smiley, J.; Lee, I.; Benkovic, S. J. *Trends Biochem. Sci.* **1994**, *19*, 145.

(3) (a) Stewart, J. D.; Benkovic, S. J. *Chem. Soc. Rev.* **1993** 213. (b) Roberts, V. A.; Stewart, J. D.; Benkovic, S. J.; Getzoff, E. D. *J. Mol. Biol.* **1994**, *235*, 1098. (c) Stewart, J. D.; Roberts, V. A.; Benkovic, S. J. *Chem. Design Automation News* **1994**, 12. (d) Stewart, J. D.; Roberts, V. A.; Thomas, N. R.; Getzoff, E. D.; Benkovic, S. J. *Biochemistry* **1994**, *33*, 1994.

(4) (a) Roberts, V. A.; Iverson, B. L.; Iverson, S. A.; Benkovic, S. J.; Lerner, R. A.; Getzoff, E. D.; Tainer, J. A. *Proc. Natl. Acad. Sci. U.S.A.* **1990**, *87*, 6654. (b) Wade, W. S.; Koh, J. S.; Han, N.; Hoekstra, D. M.; Lerner, R. A. *J. Am. Chem. Soc.* **1993**, *115*, 4449. (c) Stewart, J. D.; Roberts, V. A.; Crowder, M. W.; Getzoff, E. D.; Benkovic, S. J. *J. Am. Chem. Soc.* **1994**, *116*, 415. (d) Roberts, V. A.; Getzoff, E. D. *FASEB J.* **1995**, *9*, 94.

0002-7863/95/1517-5627$09.00/0

Scheme 1

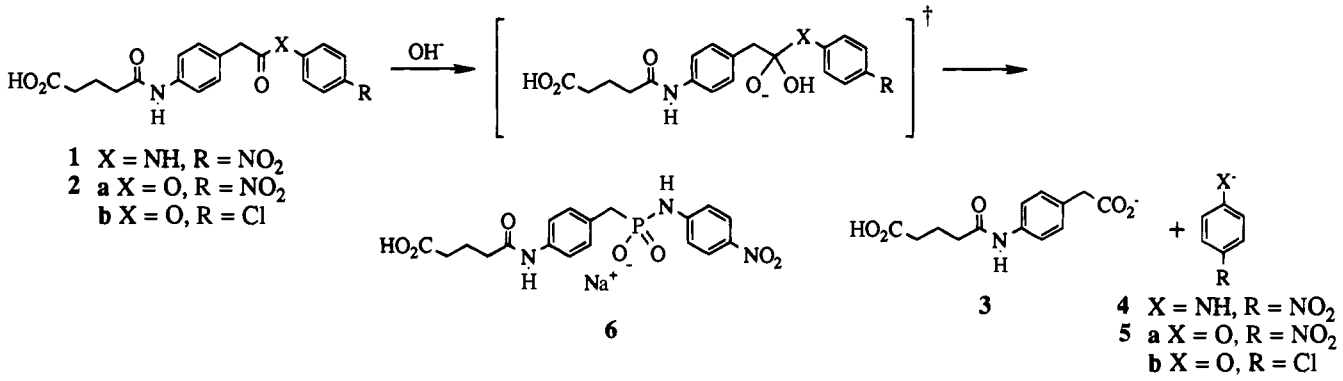

were intrigued by the potential of a metalloantibody to catalyze thermodynamically difficult reactions, in particular phosphate diester and amide cleavage. The use of metal ions to augment hydrolysis reactions is common in model systems and in naturally occurring enzymes. Metal ions appear to enhance hydrolysis reaction rates via two limiting mechanisms: (1) by acting as Lewis acids and providing positive charge for charge neutralization in transition states (hydrolysis rate increases up to 10^2) and (2) by providing a source of hydroxide, at neutral pH values, for intramolecular nucleophilic attack on a bound substrate (possible rate increases $\geq 10^4$).[5] In fact, two catalytic antibodies have been reported to require metal ions for catalysis; however, neither used a protein-coordinated metal ion directly in the catalytic process.[6] The correct juxtaposition and precise orientation of bound metal ion with substrate will be the key to the successful iterative design of a catalytic metalloantibody.[4d] We report here the design and characterization of three classes of metal ion-binding sites within the active site of an existing catalytic antibody. The results of a variety of spectroscopic studies have verified the original design.

Metal-binding sites have been introduced into antibodies by using rational mutagenesis approaches.[4,7] One promising strategy for rational design is to use crystallographic data on an existing metalloprotein and either a crystal structure or a computational model of an antibody to identify common secondary structural motifs or first sphere coordination environments possessing the proper geometry for metal ion binding. Mutagenesis is then employed to introduce metal-binding ligands into the predicted site. This approach has been successful in two antibody systems: the antifluorescein 4-4-20 antibody[4a,b] and the 43C9 single-chain antibody (SCA).[4c] In the former case several metal-binding mutants were produced; however, the wild-type form of this antibody is not a catalyst, thereby limiting its utility in testing enhanced reaction rates by coordinated metal ions. On the other hand, the 43C9 SCA has proven to be an ideal system for incorporating metal ions in the hope of enhancing the reaction rate. The antibody was raised against the phosphonamidate hapten (**6**) and can catalyze the hydrolysis of a *p*-nitroanilide compound and a series of aromatic esters (Scheme 1).[8] Both ester and amide hydrolyses are believed to proceed via a covalent acyl–antibody intermediate involving His L91.[3b,d,9] The side chain of Arg L96 is believed to stabilize the anionic transition states that flank the formation and breakdown of the acyl–antibody intermediate.[3b,d] We reasoned that placing a bound metal ion near the position occupied by the guanidinium group of Arg L96 might increase the rate of amide hydrolysis as well as open the possibility of stabilizing a pentacovalent intermediate that would form during phosphate ester hydrolysis. Both an Arg residue and Zn(II) participate in transition state stabilization by carboxypeptidase A.[10] A computer model of 43C9 SCA has been constructed, and site-directed mutagenesis studies have provided support for this model.[3b] The preparation and mutagenesis of the 43C9 SCA is very straightforward and reproducible.[3d] We have previously reported one such metal-binding derivative of 43C9, the N-H33-H, Y-H95-H double mutant, that was highly selective for Zn(II).[4c]

To date, metal binding to mutant antibodies has been ascertained by indirect fluorescence quenching experiments.[4,11] While this technique yields thermodynamic dissociation constants, it cannot verify that metal ions actually bind to the designed sites. We have therefore used a variety of spectroscopic techniques to characterize metal binding to our mutant antibodies.

Materials and Methods

General Information. The consensus nomenclature of Kabat[12] was used for numbering residues in the single-chain antibody mutants. The three CDR loops of the light chain are designated L1, L2, and L3, and those of the heavy chain are designated H1, H2, and H3. Metal ions were removed from all buffers by stirring with Chelex 100 (1 g of resin per 100 mL of buffer) for 30 min at room temperature. The resin was removed by filtration through a 0.2 μm membrane. The phosphonamidate hapten **6**, *p*-chlorophenyl ester **2b**, and acid **3** were synthesized as described previously.[8b]

Preparation of Mutants. Mutants of the 43C9 single-chain antibody were constructed with site-directed mutagenesis using the overlap extension method of Ho[13] or by cassette mutagenesis using procedures similar to those described earlier.[3d] The single-chain antibody mutants were isolated using previously published procedures.[3d] Following chromatography on Poly CAT A, the purified antibodies were concentrated by ultrafiltration (Amicon YM10 or Centricon 10) and then dialyzed against 2 × 500 mL of 100 mM HEPES, pH 7.5 containing 50 mM NaCl at 4 °C. Protein purity was ascertained by

(5) Vincent, J. B.; Crowder, M. W.; Averill, B. A. *Trends Biochem. Sci.* **1992**, *17*, 105.

(6) (a) Iverson, B. L.; Lerner, R. A. *Science* **1989**, *243*, 1184. (b) Wade, W. S.; Ashley, J. A.; Jahangiri, G. K.; McElhaney, G.; Janda, K. D.; Lerner, R. A. *J. Am. Chem. Soc.* **1993**, *115*, 4906.

(7) Gregory, D. S.; Martin, A. C. R.; Cheetham, J. C.; Rees, A. R. *Protein Eng.* **1993**, *6*, 29.

(8) (a) Janda, K. D.; Schloeder, D.; Benkovic, S. J.; Lerner, R. A. *Science* **1988**, *241*, 1188. (b) Gibbs, R. A.; Benkovic, P. A.; Janda, K. D.; Lerner, R. A.; Benkovic, S. J. *J. Am. Chem. Soc.* **1992**, *114*, 3528. (c) Gibbs, R. A.; Posner, B. A.; Filpula, D. A.; Dodd, S. W.; Finkelman, M. A. J.; Lee, T. K.; Wroble, M.; Whitlow, M.; Benkovic, S. J. *Proc. Natl. Acad. Sci. U.S.A.* **1991**, *88*, 4001.

(9) Benkovic, S. J.; Adams, J. A.; Borders, C. L.; Janda, K. D.; Lerner, R. A. *Science* **1990**, *250*, 1135.

(10) (a) Christianson, D. W.; Lipscomb, J. D. *Acc. Chem. Res.* **1989**, *22*, 62. (b) Phillips, M. A.; Fletterick, R.; Rutter, W. J. *J. Biol. Chem.* **1990**, *265*, 20692.

(11) Iverson, B. L.; Iverson, S. A.; Roberts, V. A.; Getzoff, E. D.; Tainer, J. A.; Benkovic, S. J.; Lerner, R. A. *Science* **1990**, *249*, 659.

(12) Kabat, E. A.; Wu, T. T.; Perry, H. M.; Gottesman, K.; Foeller, C. *Sequences of Proteins of Immunological Interest*, 5th ed.; National Institutes of Health: Bethesda, MD, 1991.

(13) Ho, S. N.; Hunt, H. D.; Norton, R. M.; Pullen, J. K.; Pease, L. R. *Gene* **1989**, *77*, 51.

Table 1. Thermodynamic Dissociation Constants for 43C9 Single-Chain Antibody Mutants

	mutant	plasmid	K_D values: hapten (nM)	phenol (μM)	acid (μM)	Cu(II) (μM)	Zn(II) (μM)	ref
	wild-type	pJS118	<1	0.6 ± 0.1	15 ± 1	N.Q.[b]	N.Q.	3d
class 1	Y-L32-H, A-L34-H	pJS140	>10000	>100	>300	N.Q.	3.3 ± 0.8	*a*
class 2	N-H33-H, Y-H95-H	pJS143	370 ± 20	2.5 ± 0.3	>100	N.Q.	1.54 ± 0.09	4c
	H-L91-Q, N-H33-H, Y-H95-H	pMC100	3000 ± 600	13 ± 2	>100	N.Q.	3.7 ± 0.3	*a*
	R-L96-Q, N-H33-H, Y-H95-H	pJS181	>10000	>100	>200	N.Q.	3.0 ± 0.2	*a*
class 3	R-L96-H	pMC107	520 ± 40	27 ± 3	112 ± 44	0.5 ± 0.2	10 ± 3	*a*
	R-L96-H, Y-H95-H	pMC105	3000 ± 500	5 ± 1	50 ± 10	2.1 ± 0.7	40 ± 20	*a*
	R-L96-H, Y-H95-F	pJS216	440 ± 60	2.6 ± 0.6	20 ± 10	20 ± 5	10 ± 3	*a*
	H-L91-E, R-L96-H, Y-H95-H	pMC108	2000 ± 1000	6.9 ± 1.7	80 ± 16	1.0 ± 0.2	37 ± 4	*a*

[a] This work. [b] N.Q. = no reversible quench of fluorescence observed.

SDS-PAGE, and the protein concentration was calculated using $\epsilon_{280} = 4.85 \times 10^4\ M^{-1}\ cm^{-1}$ or by fluorescence active site titrations of the antibody with hapten, **6**.[8c]

Fluorescence Titrations. Fluorescence titrations were performed at 25 °C in 100 mM HEPES, pH 7.5 containing 50 mM NaCl on an Aminco SLM 8000 spectrofluorimeter. The thermodynamic dissociation constants (K_D's) were evaluated by following the quenching of the intrinsic antibody tryptophan fluorescence at 340 nm upon excitation at 280 nm as a function of added ligand.[4c] The observed fluorescence readings were corrected for inner filter effects by the simultaneous titration of a tryptophan standard solution and for the denaturation of antibody during the titration. The degree of antibody denaturation, as indicated by a loss of fluorescence signal, was determined by titrating the antibody with buffer and subtracting the fluorescence signal decrease from all experimental data. This loss of signal intensity, due to denaturation, was found to be linear (plot of fluorescence intensity vs addition of buffer) and accounts for <10% of the total reduction of fluorescence during the course of the titration experiment. For unstable mutants, this denaturation could be reduced by the inclusion of 10% glycerol in the fluorescence buffer. The total antibody concentration in each titration was circa 200−300 nM, and whenever possible, less than the K_D of the ligand (except in the case of certain active site titrations). After addition of a concentrated antibody stock solution to the fluorescence buffer (total volume of 1 mL), the antibody was allowed to equilibrate for 15 min prior to the first addition of titrant. Small volumes (1−5 μL) of concentrated titrant made in fluorescence buffer were added to the antibody. Following corrections for antibody denaturation and inner filter effects, the corrected data were fit to a quadratic equation[4c] using the nonlinear least-squares computer program CURVE FIT v. 0.8. The errors reported in Table 1 reflect the fitting errors. The data were also replotted in Scatchard form to verify 1:1 ligand:antibody stoichiometries. For titrations involving metal ions, 500 μM EDTA was added at the conclusion of the experiment to verify that quenching was due to reversible metal binding.[4b] Typically, 50−80% of the original fluorescence returned. The inability to observe a full return of intrinsic fluorescence has been attributed to photobleaching of the antibody during the titration.[4c]

Continuous-Wave EPR Studies. X-band continuous-wave EPR spectra at liquid He temperatures were acquired on a Varian E-109 spectrometer, with a homodyne receiver, equipped with an Oxford Instruments ESR-9/10 cryostat and transfer line. Spectra were recorded and also stored as digital files using a MACLAB 4 data converter interfaced to a Macintosh computer. EPR spectra were processed (baseline subtraction and smoothing) using the program IGOR from ADInstruments (Milford, MA). Copper EPR spectra were simulated on a Silicon Graphics Indigo XZ[2] using a program written by Graeme R. Hanson (Centre for Magnetic Resonance and Department of Chemistry, University of Queensland, Queensland 4072, Australia). Typical experimental conditions: temperature, 5 K; power, 2 mW (slightly saturating); modulation amplitude, 10 G. For more concentrated samples, spectra were also recorded at 0.05 mW and 1.6 G modulation amplitude. Spectra run at liquid nitrogen temperatures were collected on a Bruker 300 E spectrometer operating at *ca.* 110 K. In all cases, the spectra were background-subtracted. The concentration of SCA was typically >100 μM, and a near stoichiometric amount of $CuCl_2$ was added to each sample.

UV−Vis Spectroscopy Studies. UV−vis spectroscopic titrations were performed on an OLIS Cary 14 or a Cary 1 spectrophotometer at 25 °C in 100 mM Na-HEPES, pH 7.5 containing 50 mM NaCl. The R-L96-H/phenol competition experiment was conducted by adding small (<5 μL) additions of $CuCl_2$ (dissolved in ddH_2O) to 100 μM R-L96-H-phenol complex (Table 1).

Pulsed EPR Studies. ^{14}N echo modulation spectra were obtained using a homebuilt pulsed EPR spectrometer.[14] A klystron source is modulated by fast switches, and the resultant low-power pulses are amplified by a pulsed traveling wave tube amplifier. Each pulse was 15 ns in duration and delivers a maximum power of 25 W. A transmission cavity[15] was used in these experiments, and the sample volume was 170 μL. Samples were typically >100 μM and made to avoid >5% uncomplexed copper at room temperature. The homodyne-detected echo amplitude was sampled by using a gated integrator. For each sample, a stimulated echo (three pulse) experiment was performed, in which the data appear as an integrated echo intensity that is plotted as a function of the temporal separation (T) between pulses 2 and 3.[16] Spectra were obtained as a Fourier transform of this time-dependent echo amplitude.

Results and Discussion

Computer Modeling and Thermodynamic K_D Measurements. The model of the light and heavy chain domains of the variable region of the 43C9 antibody[3b] provided the basis for the design of metalloantibodies. Templates from Zn(II)-binding metalloenzymes were transplanted[4a] into the 43C9 antibody model.[4d] Metal-binding sites were designed with side-chain ligands from the light chain (class 1), from the heavy chain (class 2), and from both chains (class 3) (Figure 1). Histidine ligands were used because they are excellent Cu(II)- and Zn(II)-binding groups that are common in naturally occurring metalloenzymes[17] and have worked well in other systems.[4d,18] The side-chain orientations of histidine ligands, like those of the parent 43C9 antibody model, were selected from a database of superimposed antibody structures.[3b] Except as noted below, only minor side-chain adjustments were needed to obtain typical Zn(II)−ligand bond distances 1.9−2.1 Å in the metalloantibody models. A list of mutants and their dissociation constants (K_D values) for hapten (**6**), phenol (**5a**), acid (**3**), Cu(II), and Zn(II) are given in Table 1. A representative fluorescence binding curve is shown in the supplementary material. Binding measurements of compounds **3**, **5a**, and **6** were used to probe the extent of structural perturbation of the antigen-binding site in the mutants, as in Stewart *et al.*[3d]

In agreement with analysis of the wild-type 43C9 computer model for putative metal-binding sites, no Cu(II) binding was detected for the wild-type antibody by fluorescence quenching assays. On the other hand, modeling studies[4d] predicted that

(14) McCracken, J.; Pember, S. O.; Benkovic, S. J.; Villafranca, J. J.; Miller, R. J.; Peisach, J. *J. Am. Chem. Soc.* **1988**, *110*, 1069.
(15) Mims, W. B. *Rev. Sci. Instrum.* **1974**, *45*, 1583.
(16) Mims, W. B.; Peisach, J. *J. Chem. Phys.* **1978**, *69*, 4921.
(17) (a) Glusker, J. P. *Adv. Protein Chem.* **1991**, *42*, 1. (b) Adman, E. T. *Adv. Protein Chem.* **1991**, *42*, 145. (c) Christianson, D. W. *Adv. Protein Chem.* **1991**, *42*, 281.
(18) Regan, L. *Annu. Rev. Biophys. Biomol.* **1993**, *22*, 257.

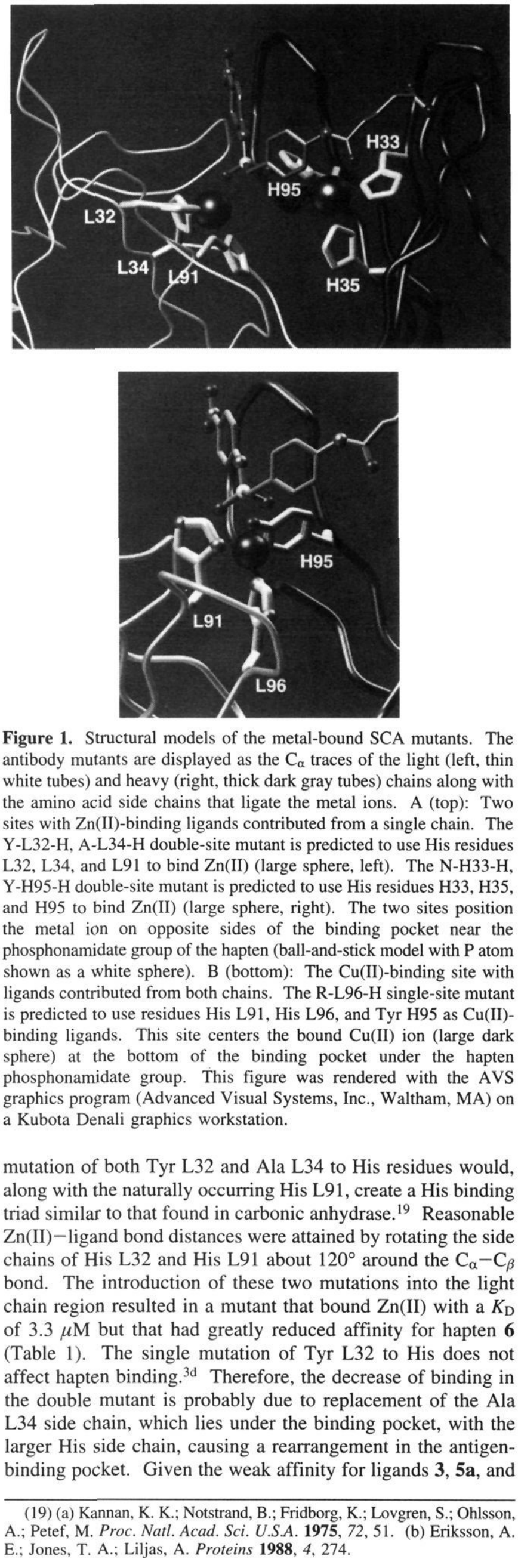

Figure 1. Structural models of the metal-bound SCA mutants. The antibody mutants are displayed as the C_α traces of the light (left, thin white tubes) and heavy (right, thick dark gray tubes) chains along with the amino acid side chains that ligate the metal ions. A (top): Two sites with Zn(II)-binding ligands contributed from a single chain. The Y-L32-H, A-L34-H double-site mutant is predicted to use His residues L32, L34, and L91 to bind Zn(II) (large sphere, left). The N-H33-H, Y-H95-H double-site mutant is predicted to use His residues H33, H35, and H95 to bind Zn(II) (large sphere, right). The two sites position the metal ion on opposite sides of the binding pocket near the phosphonamidate group of the hapten (ball-and-stick model with P atom shown as a white sphere). B (bottom): The Cu(II)-binding site with ligands contributed from both chains. The R-L96-H single-site mutant is predicted to use residues His L91, His L96, and Tyr H95 as Cu(II)-binding ligands. This site centers the bound Cu(II) ion (large dark sphere) at the bottom of the binding pocket under the hapten phosphonamidate group. This figure was rendered with the AVS graphics program (Advanced Visual Systems, Inc., Waltham, MA) on a Kubota Denali graphics workstation.

mutation of both Tyr L32 and Ala L34 to His residues would, along with the naturally occurring His L91, create a His binding triad similar to that found in carbonic anhydrase.[19] Reasonable Zn(II)−ligand bond distances were attained by rotating the side chains of His L32 and His L91 about 120° around the $C_\alpha-C_\beta$ bond. The introduction of these two mutations into the light chain region resulted in a mutant that bound Zn(II) with a K_D of 3.3 μM but that had greatly reduced affinity for hapten **6** (Table 1). The single mutation of Tyr L32 to His does not affect hapten binding.[3d] Therefore, the decrease of binding in the double mutant is probably due to replacement of the Ala L34 side chain, which lies under the binding pocket, with the larger His side chain, causing a rearrangement in the antigen-binding pocket. Given the weak affinity for ligands **3**, **5a**, and **6**, this metal-binding mutant is unlikely to be useful as a potential catalyst on substrates structurally related to the hapten.

We have previously reported a metal-binding derivative of 43C9 in which all metal ligands were located in the heavy chain region of the antibody.[4c] This mutant, N-H33-H, Y-H95-H, binds zinc selectively (K_D = 1.54 μM) over any other divalent metal ion tested and could be used as a biosensor for zinc in dilute aqueous solutions. From the design of this metal ion-binding site,[4d] His H33, His H35, and His H95 were predicted to be ligands to the Zn(II) ion. Reasonable Zn(II)−ligand bond distances were attained by rotating the solvent-exposed side chain of His H33 about 120° around the $C_\alpha-C_\beta$ bond. In this double mutant, addition of Zn(II), a diamagnetic ion, quenched 85% of the intrinsic tryptophan fluorescence. This unusual fluorescence quenching by Zn(II) may be due to side-chain contacts between metal-bound His H35 and Trp H47 or a disturbance of the conserved hydrogen bond between those same two residues.[3d,4c] In spite of three His residues acting as ligands, the K_D for Zn(II) was only micromolar; the three histidine triad in carbonic anhydrase (the basis of our design) *binds Zn(II) with a K_D of 10^{-12} M*.[20] We reasoned that other residues within the antigen-binding site might interfere with zinc binding. We also wanted to rule out any potential metal ligands, in particular His L91, that were not part of our designed metal-binding site. Mutation of this residue to Gln, to create the H-L91-Q, N-H33-H, Y-H95-H triple mutant, resulted in further weakening of hapten and phenol binding (3.0 and 13 μM, respectively), with little or no change in acid or Zn(II) binding, supporting the original design predictions. The positively charged side chain of Arg L96 might interfere with Zn(II) binding by electrostatic repulsion. Further mutation of Arg L96 to Gln, to create the R-L96-Q, N-H33-H, Y-H95-H triple mutant, resulted in a protein with similar affinity for Zn(II) (3.0 μM), but with greatly reduced affinity for ligands **5a** and **6**. These results support the computer model for Zn(II) binding to the biosensor mutant (N-H35-H, Y-H95-H 43C9 SCA). Further analysis of the initial computer model[4c] suggested that the metal is bound to one side of the antigen pocket too far from the hapten phosphonamidate group to participate directly in catalysis of structurally related substrates.

In an attempt to center the bound metal ion higher in the antigen-binding pocket, computer modeling studies were undertaken to create a metal-binding site that utilized residues from both the light and heavy chains, as well as to locate the bound metal ion near the position occupied by the Arg L96 side chain in the wild-type protein. On the basis of these considerations, we chose to substitute His for Arg L96. The model predicted that His residues at positions L91 and L96 and possibly Tyr H95 would serve as metal ligands.[4d] Slight adjustments of the His L91 and His L96 side chains provided reasonable metal−ligand bond distances and placed the Zn(II) ion 2 Å from the Tyr H95 hydroxyl group. Superimposition of the zinc-binding sites of thermolysin,[21] carbonic anhydrase I,[19a] and carboxypeptidase A[10] onto the designed metal ion-binding site revealed that the modeled site in the 43C9 SCA mutant represents a common first sphere structural motif.

Fluorescence titrations of the R-L96-H 43C9 SCA mutant with Zn(II) and Cu(II) revealed that these ions were bound with K_D values of 10 ± 3 and 0.5 ± 0.2 μM, respectively (Table 1). While the presence of the R-L96-H mutation weakened ligand binding over that observed in the wild-type protein (Table 1), the effects were not as dramatic as those previously observed for class 1 and certain class 2 mutants. The 520 nM K_D obtained for hapten should be sufficient to allow structurally-related, potential substrates to bind.

(19) (a) Kannan, K. K.; Notstrand, B.; Fridborg, K.; Lovgren, S.; Ohlsson, A.; Petef, M. *Proc. Natl. Acad. Sci. U.S.A.* **1975**, *72*, 51. (b) Eriksson, A. E.; Jones, T. A.; Liljas, A. *Proteins* **1988**, *4*, 274.

(20) Lindskog, S.; Malmstrom, B. G. *J. Biol. Chem.* **1962**, *237*, 1129.
(21) Holmes, M. A.; Matthews, B. M. *J. Mol. Biol.* **1982**, *160*, 623.

We explored a number of additional mutations designed to reveal the ligands used for binding of metal ions. Substitution of Phe for Tyr H95 resulted in a double mutant, R-L96-H, Y-H95-F, that showed no reduction in the K_D value for Zn(II) over that seen in the R-L96-H mutant, but a 40-fold weakening of Cu(II) binding (Table 1). These results suggested that Zn(II) and Cu(II) are both bound by His L91 and His L96 and that Cu(II) is, in addition, bound by the phenolic oxygen of Tyr H95. This participation in Cu(II) binding is supported by UV−vis measurements (*vide infra*). We attempted to improve metal binding by introducing an additional His at position H95. Unfortunately, the double mutant (R-L96-H, Y-H95-H) displayed a 4-fold reduction in its affinity for both Zn(II) and Cu(II) compared to the single mutant (Table 1). These modest reductions in metal ion binding are likely a result of subtle alterations in the protein geometry imposed by the Tyr to His substitution. We attempted to increase the affinity of the site for metal ions by introducing charge complementarity by substituting Glu for His L91 in the R-L96-H, Y-H95-H double mutant. However, the metal ion-binding properties of this triple mutant were nearly the same as those of the R-L96-H, Y-H95-H double mutant although the affinity for hapten was decreased by ca. 4-fold as compared to the R-L96-H single mutant (Table 1). Our observations parallel those observed previously for carbonic anhydrase II, where the replacement of His by Asp resulted in a 10^4 loss of protein-Zn(II) affinity, even though the three-dimensional structure of the mutant revealed a normal carboxylate−Zn(II) interaction.[22]

Continuous-Wave (CW) EPR Studies. Since our only evidence for metal binding to these SCA mutants was the quenching of the intrinsic tryptophan fluorescence, we sought more direct evidence for metal binding. Zn(II) is a d^{10} metal ion that is spectroscopically silent; however, the fact that Cu(II) binds to certain mutants of the 43C9 SCA provided us with a means to directly probe metal binding. Since Zn(II) and Cu(II) can sometimes replace one another in naturally-occurring metalloenzymes,[23] information on the binding sites gleaned from studies on the Cu(II)-bound forms would be applicable to Zn(II) binding as well. However, metal coordination geometries of Cu(II) and Zn(II) may vary in the same site,[24] as suggested by differential metal-binding results (Table 1) on the Tyr H95 to Phe mutant in the class 3 site.

We have examined the CW-EPR spectra of all of the metal-binding mutants of 43C9 SCA. The overall shapes and positions of the crossover points ($g_\perp$ region at $g \approx 2.0$) of all spectra were essentially identical (data not shown); however, there were noticeable shifts of features in the $A_\parallel$ region (Figure 2 and Table 2). Spectra of the non-Cu(II)-binding mutants (wild-type 43C9 SCA; N-H33-H, Y-H95-H; H-L91-Q, N-H33-H, Y-H95-H; R-L96-Q, N-H33-H, Y-H95-H) showed two dominant features in the $A_\parallel$ region at $g = 2.44$ and 2.30 with apparent $g_\parallel = 2.23$ (Figure 2, bottom). On the other hand, the binding of Cu(II) to the Cu(II)-binding mutants (R-L96-H; R-L96-H, Y-H95-H; H-L91-E, R-L96-H, Y-H95-H) resulted in spectra with increased intensity at $\sim g = 2.40$ and $g = 2.27$, in addition to the intensity seen in the nonbinding mutants (Figure 2, top). The apparent $A_\parallel$ values (>160 G) suggest type II-like Cu(II) binding sites with nitrogen and/or oxygen ligands (typical $A_\parallel$ values >100 G) rather than type I Cu(II)-like centers (typical values <100 G).[25]

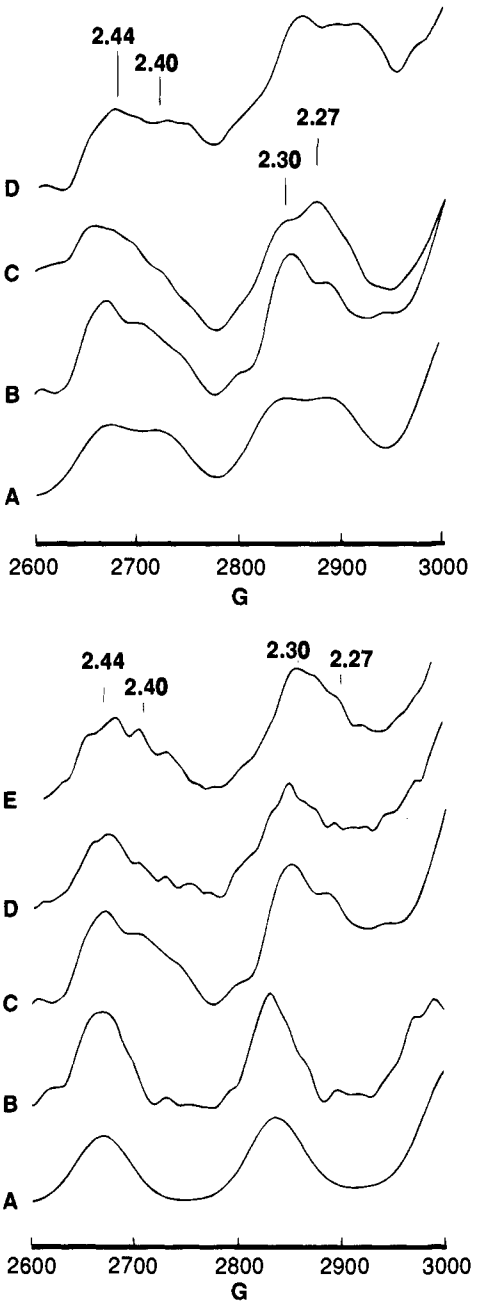

Figure 2. EPR spectra of Cu(II) and 43C9 SCA mutants at 5 K in the $A_\parallel$ region. (Top panel) Metal-binding mutants of 43C9 SCA: (A) simulated spectrum of 53% unbound Cu(II) and 47% bound Cu(II) using parameters in Table 2; (B) 222 μM wild-type 43C9 SCA and 222 μM Cu(II); (C) 258 μM R-L96-H SCA and 258 μM Cu(II); (D) 46 μM R-L96-H, Y-H95-H SCA and 46 μM Cu(II). (Bottom panel) Non-Cu(II)-binding mutants of 43C9 SCA: (A) simulated spectrum of free Cu(II) using parameters in Table 2; (B) 167 μM Cu(II); (C) 222 μM wild-type 43C9 SCA and 222 μM Cu(II); (D) 150 μM N-H33-H, Y-H95-H SCA and 150 μM Cu(II); (E) 78 μM R-L96-Q, N-H33-H, Y-H95-H SCA and 78 μM Cu(II). All samples were degassed before freezing. Typical operating conditions: scan range, 2000 G; field center, 3200 G; time constant, 0.250 s; scan time, 30 min; modulation amplitude, 10 G; modulation frequency, 100 kHz; receiver gain, 2×10^4; microwave power, 2 mW; microwave frequency, 9.225 GHz.

We have used the ratios of intensities at $g = 2.27$ to those at $g = 2.30$ to evaluate the differences in the EPR spectra of the binding and nonbinding mutants (Table 2). A simulation

(22) Kiefer, L. L.; Ippolito, J. A.; Fierke, C. A.; Christianson, D. W. *J. Am. Chem. Soc.* **1993**, *115*, 12581.

(23) Bertini, I.; Luchinat, C.; Scozzafava, A. *Struct. Bonding* **1982**, *45*, and references therein.

(24) (a) Häkansson, K.; Wehnert, A.; Liljas, A. *Acta Crystallogr.* **1994**, *D50*, 93. (b) Nar, H.; Huber, R.; Messerschmidt, A.; Filippou, A. C.; Barth, M.; Jaquinod, M.; van de Kamp, M.; Canters, G. W. *Eur. J. Biochem.* **1992**, *205*, 1123.

(25) Peisach, J.; Blumberg, W. E. *Arch. Biochem. Biophys.* **1974**, *165*, 691.

Table 2. Apparent CW EPR Parameters at 4 K

sample	$g_\perp$	$g_\parallel$	$A_\parallel$ (G)	2.27/2.30[a]
wild type	2.06	2.23	170	0.84
R-L96-H	2.07	2.19	170	1.075
R-L96-H, Y-H95-H	2.06	2.20	169	1.16
N-H33-H, Y-H95-H	2.05	2.23	173	0.68
Cu(II)	2.07	2.26	168	0.09
R-L96-Q, N-H33-H, Y-H95-H	2.05	2.21	180	0.92

[a] Intensity ratio of the $g = 2.27$ and $g = 2.30$ features.

Table 3. Simulated Parameters of the 4 K CW EPR Spectra[a]

	$A_\parallel$ (G)	$A_\perp$ (G)	$g_\parallel$	$g_\perp$	line width$_\parallel$ (G)	line width$_\perp$ (G)
free Cu(II)	167.9	6.0	2.23(8)	2.05	33	26
bound Cu(II)	166.0	6.0	2.19(6)	2.05	33	26

[a] Microwave frequency in simulation was 9.155 GHz.

composed of 53% of a spectrum with features of the new intensity in the binding mutants ($A_\parallel = 166.0$ G, $A_\perp = 6.0$ G, $g_\parallel = 2.19$, and $g_\perp = 2.05$) and 47% of a spectrum similar to that obtained from Cu(II) in buffer ($A_\parallel = 167.9$ G, $A_\perp = 6.0$ G, $g_\parallel = 2.23$, and $g_\perp = 2.05$) gives a ratio of intensities at these g values of 1.0 (Figure 2A, top). The simulation parameters represent average features of the experimental spectra of the two mutants (R-L96-H and R-L96-H, Y-H95-H) which were shown by fluorescence to bind copper (Figure 2C,D, top). The ratio of intensities at $g = 2.27$ and 2.30 is greater than 1.0 for these mutants (Table 2). Two other mutants, which show no evidence of copper binding by fluorescence quenching, give lower, but significant, ratios of these intensities in the CW-EPR. These are the wild-type SCA (Figure 2B, top) and the triple, zinc-binding mutant (R-L96-Q, N-H33-H, Y-H95-H; Figure 2E, bottom). These results suggest that at the high protein and copper concentrations used for EPR (>45 μM), weak or nonspecific metal-binding sites with K_D values >100 μM may be significantly populated and may give the same EPR spectra as the mutants with higher affinity. In typical fluorescence titrations, the SCA concentration was ca. 300 nM and the highest concentration of Cu(II) that could be used was <100 μM at 23 °C as a result of inner filter effects. The presence of a weak metal-binding site on the wild-type SCA is supported by the observation of slight inhibition of wild-type 43C9 SCA-catalyzed hydrolysis of the *p*-chlorophenyl ester substrate (**2b**) in the presence of metal ions (22 and 17% inhibition of 2 μM SCA in the presence of 20 μM Cu(II) and 30 μM Zn(II), respectively). For the triple, zinc-binding mutant, it is not surprising that Cu(II) may bind to the Zn(II) site with 2 orders of magnitude less affinity under the EPR conditions. The significant contribution of EPR signals resembling those of Cu(II) in buffer in all samples may be the result of phase separations during freezing or of weak binding sites that give a spectrum very similar to that of copper in buffer. Lastly, sufficient quantities of the H-L91-E, R-L96-H, Y-H95-H 43C9 SCA triple mutant were not available for EPR spectroscopy.

Pulsed EPR (Electron Spin Echo Envelope Modulation) Studies. Since CW EPR studies could not verify that Cu(II) bound specifically to histidines in the genetically engineered binding site, we turned to electron spin echo envelope modulation (ESEEM) studies for this type of information. In Cu(II)-histidine complexes, ESEEM spectra are sensitive to the weakly-coupled nonbonding ^{14}N of the imidazole side chain. Generally, these spectra are characterized by a pair of intense features below 2 MHz that correspond to nuclear quadrupole transitions (Figure 3) and a third line appearing near 4 MHz that arises

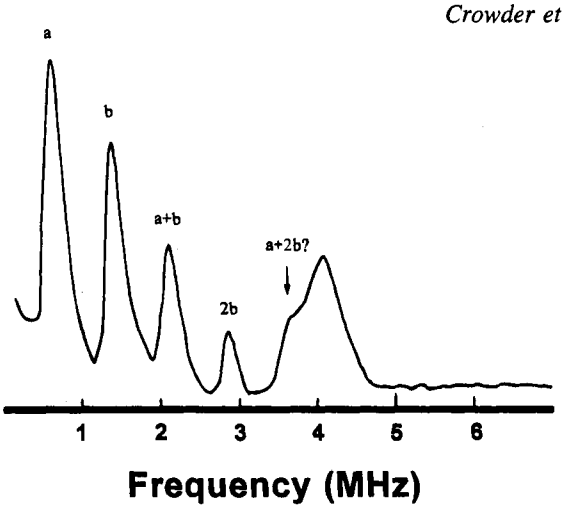

Figure 3. Fourier-transformed spectrum of Cu(imid)$_4$I$_2$. Measurement conditions: microwave frequency, 9.0210 GHz; field strength, 3100 G; microwave pulse power, 3 W; τ value, 152 ns; sample temperature, 4.2 K; pulse sequence repetition rate, 100 Hz.

from a double quantum ($\Delta M = 2$) transition.[16,26] The latter feature includes contributions from nuclear Zeeman, Fermi contact, and nuclear quadrupole terms, but probably does not contain contributions from the $\Delta M = 1$ transition because this transition is typically not resolved in powder spectra.[27]

Pulsed EPR studies supported the original design of the metal ion-binding sites. The three major "fingerprint" features were observed in the wild-type 43C9 SCA-Cu(II) spectrum (Figure 4A), which revealed coordination of Cu(II) by a single His residue. The presence of a single histidine ligand, probably His L91, is consistent with the CW-EPR prediction that some Cu(II) bound to the wild-type SCA at the high protein concentrations employed in the EPR experiments.

We observed changes in the ESEEM spectrum as the copper-binding site was modified by the addition of more histidines. When two or more equivalent nitrogen atoms are coupled to an unpaired electron spin, so-called "combination lines" appear in the FT-ESEEM spectrum as low-intensity features at the beat frequencies of the major quadrupole features (a and b) described above (Figure 3).[27a] For example, in a frozen ethanolic glass containing copper tetraimidazole, combination lines appear at twice the frequency of the fundamental lines (2b), the sum of the two fundamental lines (a + b), and the sum of the larger second harmonic and the smaller of the two fundamental lines (a + 2b) (Figure 3). Similar combination lines have been previously observed in the ESEEM spectra of several copper proteins.[14,28] The intensity, number, and frequency of these combination lines depends on the number of equivalent nuclei that are coupled to the unpaired electron spin. According to Mims,[27a] they arise from harmonic terms in the density matrix formalism that defines the echo modulation process; however, the variations observed among combination lines among proteins and other low-symmetry complexes suggests that a process analogous to symmetry breaking among coupled oscillators may be the underlying cause.

In the spectrum of the R-L96-H 43C9 SCA-Cu(II) complex, we observed weak lines at approximately 2 and 2.5 MHz (Figure 4B) that are absent in the spectrum of the wild-type + Cu(II) protein. Moreover, there is a suggestion of a third weak line that appears as a shoulder on the low-frequency side of the

(26) Jiang, F.; McCracken, J.; Peisach, J. *J. Am. Chem. Soc.* **1990**, *112*, 9035.
(27) (a) Mims, W. B. *Phys. Rev.* **1972**, *5*, 2409. (b) Colaneri, M. J.; Peisach, J. *J. Am. Chem. Soc.* **1992**, *114*, 5335.
(28) (a) Kosman, D.; Peisach, J.; Mims, W. B. *Biochemistry* **1980**, *19*, 1304. (b) Jiang, F.; Peisach, J.; Ming, L. J.; Que, L.; Chen, V. J. *Biochemistry* **1991**, *30*, 11437. (c) Balasubramanian, S.; Carr, R. T.; Bender, C. J.; Peisach, J.; Benkovic, S. J. *Biochemistry* **1994**, *33*, 8532.

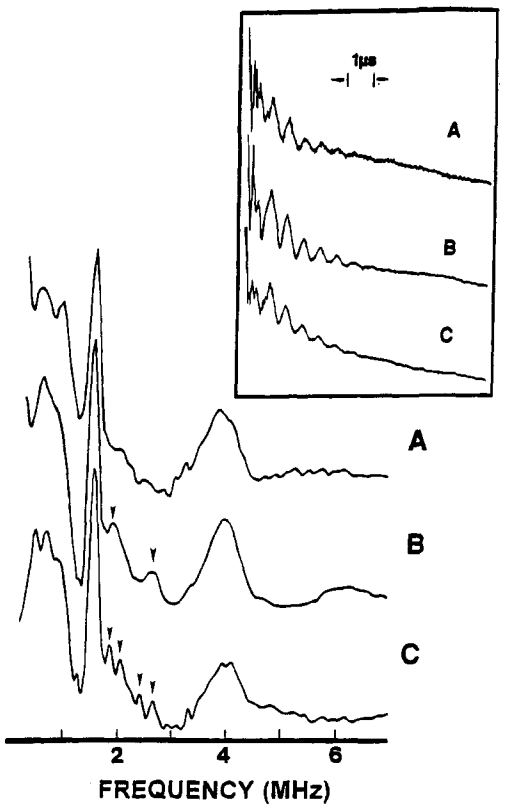

Figure 4. Fourier-transformed electron spin echo spectra: (A) 524 μM wild-type 43C9 SCA and 395 μM Cu(II); (B) 305 μM R-L96-H 43C9 SCA and 271 μM Cu(II); (C) 230 μM R-L96-H, Y-H95-H 43C9 SCA and 200 μM Cu(II). Inset: Time domain ESEEM spectra of (A) wild-type 43C9 SCA, (B) R-L96-H 43C9 SCA, and (C) R-L96-H, Y-H95-H 43C9 SCA−Cu(II) complexes. FT spectra were constructed using a method of Mims.[16] Spectral conditions are the same as described in Figure 3.

double quantum peak (at about 3.2 MHz). The low-frequency quadrupole-derived feature in the spectrum is broadened and appears to be an unresolved doublet. We therefore assign the 2 MHz feature to a combination line of the intense 1.5 MHz feature and the sharp edge of the low-frequency component (near 0.5 MHz). There is also probably some contribution from the second harmonic of the 1 MHz shoulder. The 2.5 MHz feature is a combination of the 1.5 MHz feature and the high-frequency side of the low-frequency quadrupole line (shoulder at about 1 MHz). The 2.5 MHz line is very well resolved above noise and free from the sloping baseline of adjoining spectral lines. The presence of this feature is the best evidence for a combination line in the R-L96-H + Cu(II) spectrum. We therefore infer that the introduction of a histidine at position L96 provided a second ligand to Cu(II), as predicted by computer modeling studies and suggested by the tight binding of Cu(II) to this single mutant (Table 1).

The double mutation, R-L96-H, Y-H95-H, yielded an unusual ESEEM spectrum, in the sense that the resolution is retained among the combination lines. The low-frequency quadrupole feature further splits and appears to be a triplet in the range 0.5−1 MHz. This is accompanied by a splitting of the combination lines that were previously identified in the spectrum of the R-L96-H 43C9 SCA−Cu(II). We observed one doublet at about 2 MHz and a second at 2.5 MHz. It also appears that the previously unresolved shoulder at 3.2 MHz is also split (Figure 4C). These results are consistent with the conclusion that the R-L96-H, Y-H95-H 43C9 SCA−Cu(II) complex has three histidine ligands to the Cu(II). Surprisingly, the 1.5 MHz feature is not broadened or perturbed in any of the samples. This feature is usually assigned to the ν_+ quadrupole transition and is defined by e^2Qq and η, the nuclear quadrupole interaction and the asymmetry parameter, respectively.[26] The change in the low-frequency component implies that the Y-H95-H imidazole nitrogen has a different e^2Qq or a different η, which should be likewise manifest as a change in the high-frequency feature. The overall line width in the low-frequency region does not change; therefore, the observed differences are probably not significant. The resolution in the spectrum of the R-L96-H, Y-H95-H 43C9 SCA mutant is either fortuitous or suggests a very slight variation in η.

UV−Visible Spectroscopy. The presence of three histidine ligands in the Cu(II)-bound R-L96-H, Y-H95-H double mutant and the relatively tight binding of R-L96-H to Cu(II) suggested that the R-L96-H 43C9 SCA mutant might also have a third metal ligand. Modeling studies predicted that Tyr H95 might be oriented correctly to serve as a ligand to Cu(II). In biological systems, the Cu(II)−tyrosine linkage is uncommon; however, tyrosine does serve as a ligand to Cu(II) in galactose oxidase[29] and possibly in cytochrome bo_3 ubiquinol oxidase from *Escherichia coli*.[30] In galactose oxidase, there are two ligating tyrosines: one of which (Tyr 272) is covalently bound at C_ϵ to the sulfur atom of Cys 228 forming a novel thioether bond and the other is bound apically.[31] The tyrosine−Cu(II) linkages do account for a LMCT band at 445 nm with an extinction coefficient of 5400 M^{-1} cm^{-1}. We were interested in determining whether a similar LMCT band might be observable in the R-L96-H−Cu(II) adduct.

Under our buffer conditions, free Cu(II) has an absorption maximum at ca. 675 nm. Upon addition of excess R-L96-H SCA to ensure <5% unbound Cu(II), there is a blue shift of the Cu(II) absorption band to ca. 600 nm with a concomitant increase in intensity (Figure 5, top). The same shift was observed when bovine serum albumin is used instead of the R-L96-H mutant (data not shown). The addition of R-L96-H, Y-H95-F mutant to the Cu(II) solution, again, results in a similar blue shift. The spectrum of this SCA−Cu(II) complex is nearly Gaussian with an absorption maximum at 600 nm and a small shoulder at 675 nm which is probably due to uncomplexed Cu(II) (see K_D's for Cu(II) of these two mutants in Table 1). On the other hand, while the spectrum of the R-L96-H−Cu(II) complex also shows a main peak with an absorption maximum at 600 nm, it has a shoulder at ca. 500 nm. Subtraction of the R-L96-H, Y-H95-F 43C9 SCA−Cu(II) spectra from that of the R-L96-H 43C9 SCA−Cu(II) species (after normalizing each spectrum by dividing by the $[Cu(II)]_T$) resulted in a peak with a maximum at 490 nm and an extinction coefficient of 55 M^{-1} cm^{-1} (Figure 5, bottom). We believe that this feature is the Tyr → Cu(II) LMCT band. We predict that the absence of the electron-donating thioether bond, that is present in galactose oxidase,[31] would result in a less intense, lower energy LMCT and hence a lower extinction coefficient and a shift to a higher wavelength. In addition, the modeling studies predicted that the geometry of the Y-H95 might not be optimal for strong bonding.

We also sought to determine whether metal ion would bind to the R-L96-H SCA in the presence of *p*-nitrophenol without disturbing the affinity of the latter. A similar approach was used to characterize the simultaneous binding of Zn(II) and **5a** to the N-H33-H, Y-H95-H 43C9 SCA.[4c] The binding of **5a** to the R-L96-H SCA mutant resulted in a red-shift of the phenol absorption maximum from 404 to 412 nm. The data are most

(29) Whittaker, M. M.; DeVito, V. L.; Asher, S. A.; Whittaker, J. W. *J. Biol. Chem.* **1989**, *264*, 7104.
(30) Thomas, J. W.; Calhoun, M. W.; Lemieux, L. J.; Puustinen, A.; Wilström, M.; Alben, J. O.; Gennis, R. B. *Biochemistry* **1994**, *33*, 13013.
(31) Ito, N.; Phillips, S. E. V.; Stevens, C.; Ogel, Z. B.; McPherson, M. J.; Keen, J. N.; Yadav, K. D. S.; Knowles, P. F. *Nature* **1991**, *350*, 87.

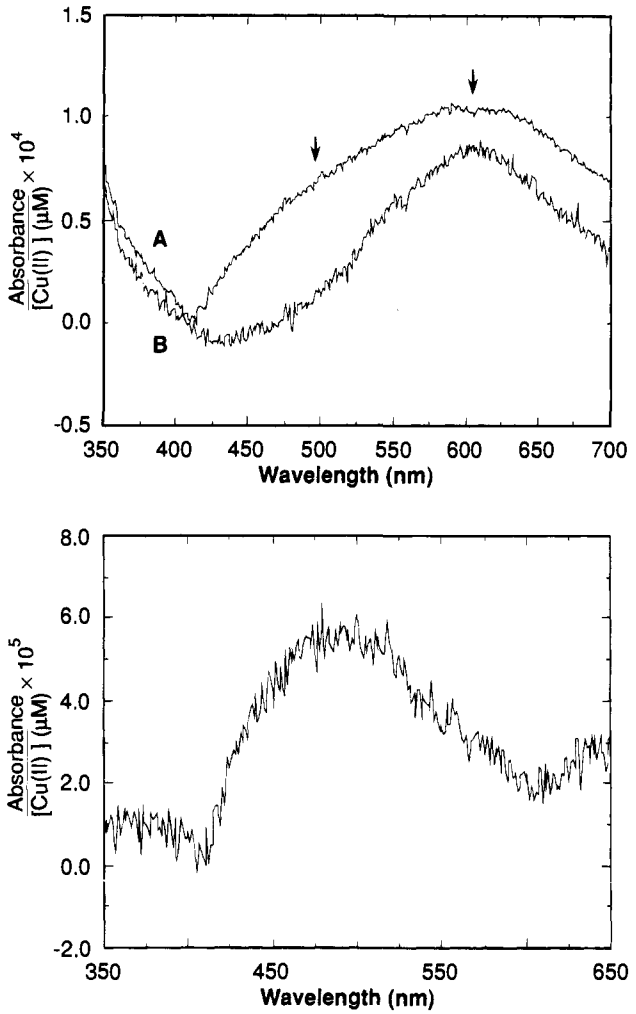

Figure 5. UV−vis spectra of Cu(II)-binding mutants. Top: (A) 100 μM R-L96-H 43C9 SCA and 90 μM Cu(II) and (B) 69 μM R-L96-H, Y-H95-F 43C9 SCA and 30 μM Cu(II). Bottom: Difference spectrum of spectrum A minus spectrum B. Both spectra were collected in 100 mM HEPES, pH 7.5 containing 50 mM NaCl. The two samples were buffer subtracted and normalized for Cu(II) by dividing the absorbance by the total concentration of added Cu(II).

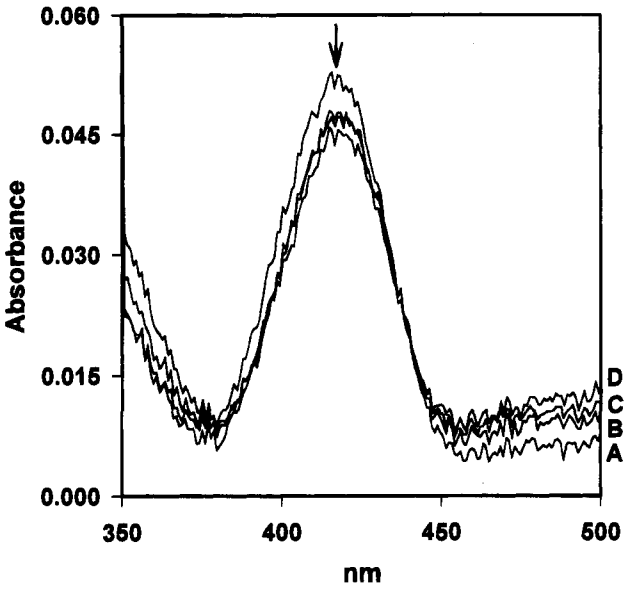

Figure 6. UV−vis difference spectra of *p*-nitrophenol-R-L96-H 43C9 SCA upon addition of Cu(II): (A) 60 μM R-L96-H and 10 μM *p*-nitrophenol; (B) 69 μM R-L96-H, 10 μM *p*-nitrophenol, and 17 μM Cu(II); (C) 69 μM R-L96-H, 10 μM *p*-nitrophenol, and 33 μM Cu(II); (D) 69 μM R-L96-H, 10 μM *p*-nitrophenol, and 150 μM Cu(II). Spectra of free *p*-nitrophenol, 69 mM unbound R-L96-H SCA, and buffer were subtracted from spectra A−D. The buffer used in this experiment was 100 mM HEPES, pH 7.5 containing 50 mM NaCl.

easily visualized in a difference spectrum (i.e., spectrum of SCA·*p*-nitrophenol minus spectra of SCA, free *p*-nitrophenol, and buffer, Figure 6). We subtracted the free *p*-nitrophenol from the spectrum because under the conditions used for the experiment, only ca. 70% of the *p*-nitrophenol was bound. The addition of 10-fold excess of Cu(II) over the calculated concentration of the SCA·*p*-nitrophenol complex did not result in a shift of the phenol absorption peak back to 404 nm (Figure 6). A control experiment demonstrated that the spectrum of Cu(II)−phenol mixture in solution was superimposable on that of the free phenol (data not shown). We interpret this result as indicating the simultaneous binding of Cu(II) and *p*-nitrophenol to the SCA. This conclusion is further supported by a fluorescence experiment performed on the R-L96-H, Y-H95-H 43C9 SCA using **5a** and Zn(II). The addition of *p*-nitrophenol to the SCA−Zn(II) complex resulted in further fluorescence quenching with a K_D for *p*-nitrophenol of 6 μM (data not shown), which matches the K_D (5 μM) for *p*-nitrophenol measured in the absence of Zn(II) (Table 1).

Conclusions

These results provide the first comprehensive spectroscopic characterization and verification of metal-binding sites in an antibody scaffold. The metal-binding sites were rationally designed using computer modeling techniques, without the aid of a crystal structure of the wild-type protein. This design predicted three novel metal-binding sites, all of which were shown to bind metal ions by fluorescence quenching. By EPR and ESEEM, we identified a low-affinity Cu(II)-binding site with a single His ligand in the wild-type 43C9 SCA. Consistent with the computational design, ESEEM spectroscopy demonstrated that the Cu(II)-binding class 3 mutants, R-L96-H and R-L96-H, Y-H95-H, have two and three His ligands, respectively. In addition, the R-L96-H mutant included an unusual Tyr ligand, as indicated by an LMCT band. For the two mutants tested, metal binding does not preclude binding of end product *p*-nitrophenol. The next step is to screen these metal-binding mutants for catalytic activity, and these studies are in progress. We are also currently attempting to study these mutants with protein crystallography in hopes of better understanding the relative positions of metal and hapten (substrates).

Acknowledgment. This work was supported by grants from the Office of Naval Research (N00014-91-J-1885 to E.D.G. and N00014-91-J-1593 to S.J.B.) and the National Institutes of Health (GM 48877 to V.A.R.; RR 02538 to J.P.; GM 48495 to E.D.G.; GM 36232 to B.J.G.) and by post-doctoral fellowships from Helen Hay Whitney Foundation (J.D.S.) and National Institutes of Health (M.W.C., GM 16049). The authors would like to thank M. E. Pique for help with computer graphics.

Supplementary Material Available: A representative fluorescence titration curve of R-L96-H 43C9 SCA with hapten (1 page). This material is contained in many libraries on microfiche, immediately follows this article in the microfilm version of the journal, can be ordered from the ACS, and can be downloaded from the Internet; see any current masthead page for ordering information and Internet access instructions.

JA943596X